

## ANALYSIS OF A PNEUMATIC BAND BRAKING SYSTEM FOR INDUSTRIAL WINCHES

Georgiana-Alexandra MOROȘANU<sup>1</sup>, George-Ștefan LEOCA<sup>2,3</sup>,  
Doina BOAZU<sup>3</sup>, Nicușor BAROIU<sup>4</sup>

<sup>1</sup> Department of Continuous Training and Technological Information, Danubius International University of Galati, Romania, georgianaalexandra.morosanu@univ-danubius.ro

<sup>2</sup> DMT Marine Equipment, Galati, Romania  
george.leoca@yahoo.com

<sup>3</sup> Department of Mechanical Engineering, "Dunarea de Jos" University of Galati, Romania  
Doina.Boazu@ugal.ro

<sup>4</sup> Department of Manufacturing Engineering, "Dunarea de Jos" University of Galati, Romania  
Nicusor.Baroiu@ugal.ro

**Abstract:** Band braking systems are widely used in industrial and marine mechanisms due to their efficiency in generating braking moment through friction between the brake band and the rotating drum. These systems have a simple construction, consisting of a metal band covered with a friction material (ferodo), which tightens around a drum in order to reduce the rotation speed or to completely stop the mechanism. The analysis of these systems is frequently performed using the finite element method (FEM), which allows the assessment of the distribution of stresses and strains in the structural elements. CAD methods are essential in the accurate modeling of braking components, and the use of CAE-type software for static and dynamic simulation provides a detailed assessment of mechanical performance, including von Mises stress distribution and the safety factor. The paper presents a study on the band braking system from the structure of industrial winches. The design of this system was realized through CAD modeling using Autodesk Inventor software, which allowed the precise creation of the geometry of the system components, such as the brake band, pneumatic cylinders and support elements. Based on this modeling, finite element method (FEM) simulations were performed in Ansys Workbench for both static and dynamic analysis. Static analysis was used to assess the stress and strain distribution in the system components, while dynamic analysis simulated the operating conditions during rapid braking. In addition, the paper includes analytical calculations in order to verify the strength of various components, such as joints and welds, which are used to validate the design and to compare with the results obtained from numerical simulations.

**Keywords:** Band brake, pneumatic cylinder, CAD, resistance calculation, Ansys Workbench, FEM, mesh

### 1. Introduction

Mechanisms are provided with braking devices that aim to stop the movement of the load, the mobile part of the mechanism or the entire mechanism and keep them safely in a position of static balance. These braking subassemblies operate on the principle of friction braking and convert mechanical energy into heat energy, which is dissipated into the environment. The construction of the braking devices must be simple and robust, allow easy adjustment and have the smallest possible dimensions. As a rule, the braking elements are installed directly on the shaft connected to the motor, where the external forces generate the smallest moments. In the design of such elements, both kinematic and dynamic parameters must be taken into account, as well as the number of brakings per time unit in which cases the braking moment and the method of exhausting caloric energy must be taken into account in the imposed admissible values. Band brakes have as a specific element a braking band made up of a metal part and a ferodo part, a material with a high friction coefficient. The tape wraps around the brake wheel at an angle of about 250° [1, 2, 3].

In the case of the present paper, the braking band consists of two parts, connected at two of the ends by a joint element and connected at the other ends by the rigid body of the brake. In the structure of the brake is a lever directly connected to the band brake, which, once actuated in one

direction, produces the tightening necessary for braking, and in the other direction produces the relaxation of the assembly. It should be noted that the auxiliary element of the drum on which the band brake is placed is called the brake track. This element has a cylindrical shape of small length compared to its diameter, the inner face and the outer face being processed in such a way as to ensure braking under conditions required by operation [4, 5].

By operating conditions it is understood that the brake must provide a maximum braking force imposed in the design, a force which, once defeated, must lead to a decoupling of the braking element. This condition is mandatory to prevent destruction of the braking system.

Braking systems are mounted on the outer surface of the braking track, the inner track being used for couplings that transmit the moment transmitted by the engine to the shaft and from the shaft to the drum [4, 5]. Figure 1 shows the braking path mounted on the drum of a winch [6].

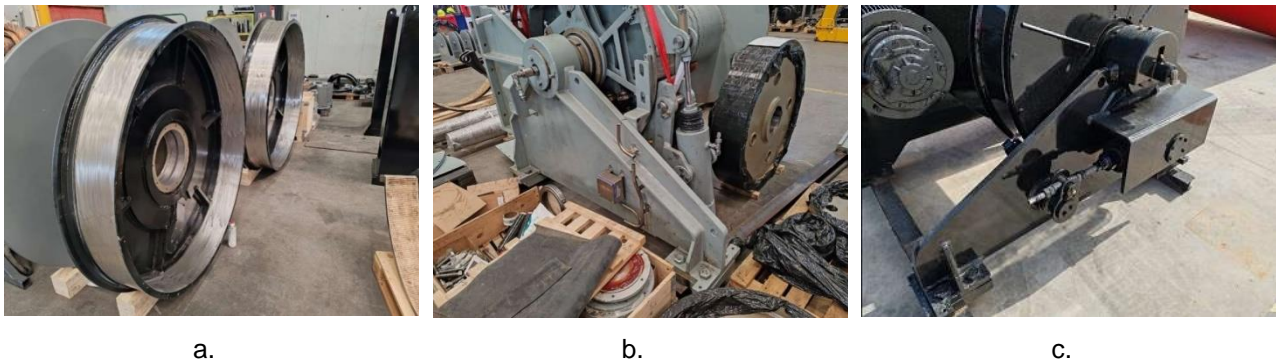


**Fig. 1.** Braking systems:  
brake track on drum (a); vertical braking system (b); horizontal braking system (c) [6]

From the point of view of the discharge of the forces generated in the brake body, traction and compression brakes are distinguished. These types of brakes are distinguished by the way the cable is wrapped on the drum. Figure 2 shows the forces, moments and reactions occurring within the braking system. It should be noted that reactions occur in the welding area on board brake vessel.

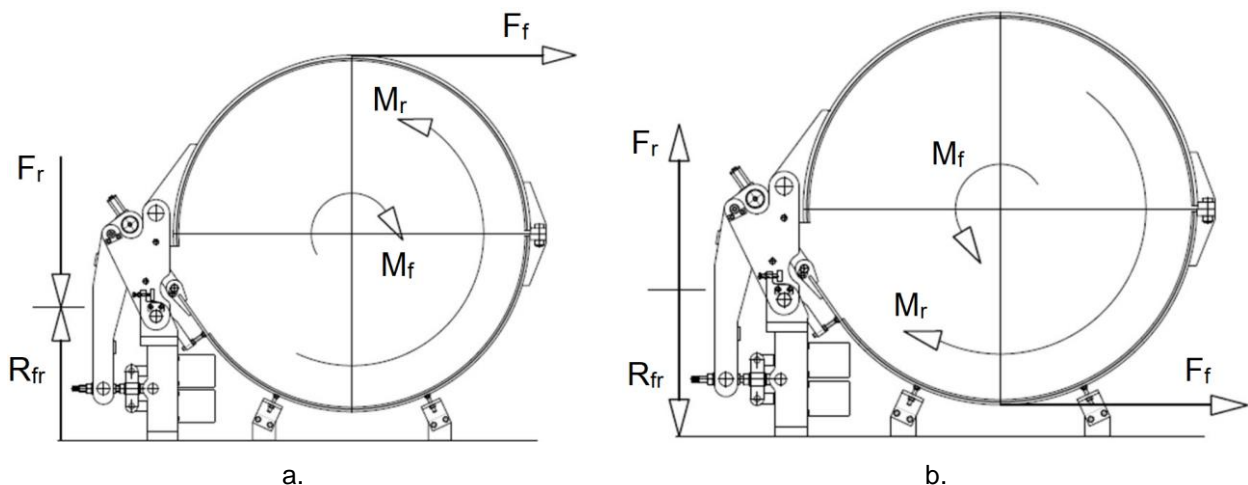


**Fig. 2.** Schematic of a traction (a) and compression (b) brake [6]

It is observed that in the case of the two brakes, the braking force  $F_f$  generated in the system is represented, which creates a braking moment  $M_f$ . The reaction moment  $M_r$ , which opposes the braking moment due to static balance, generates a reaction force  $F_r$ , which is equaled by a ground reaction  $R_{fr}$ .

Also, the orientation of the  $R_{fr}$  reaction gives the name of the brake type: if the reaction is oriented as in Figure 2.a, it generates tensile stresses (hence the traction brake name), and if it is oriented as in Figure 2.b, this generates compression stresses on board the ship, hence the compression brake name.

Figure 3 shows the diagram of a band brake.

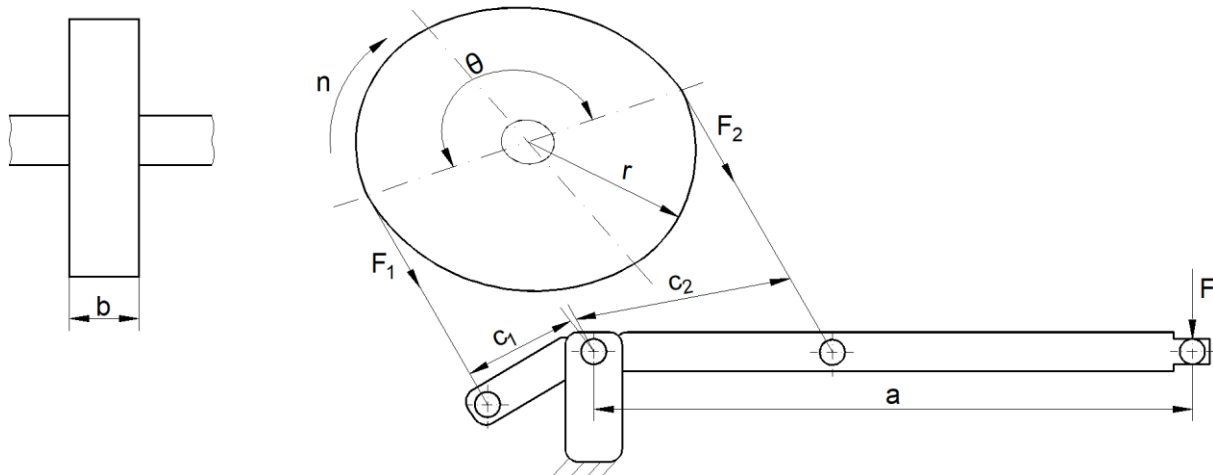


Fig. 3. General case of a band brake - working diagram [6]

Band brakes have in their structure a disc mounted on a shaft, a metal band that enwraps a certain portion of the disc, the metal band that is lined with ferodo in order to increase friction and a lever that can oscillate around a fixed point. The ends of the tape are fixed on the lever. If the lever rotates in a certain direction, the band is pressed against the disc and therefore the brake is tightened. Rotation in the other direction weakens the brake action. The  $F$  force required for braking is calculated with relation (1) [6]:

$$F = \frac{F_2 \cdot c_2 - F_1 \cdot c_1}{a} = F_2 \cdot (c_2 - c_1 \cdot e^{\mu \cdot \theta}) [\text{N}]; \quad F_1 = F_2 \cdot e^{\mu \cdot \theta} [\text{N}] \text{ (Euler)}, \quad (1)$$

where:  $F$  represents the applied force;  $n$  - shaft speed, in rpm;  $a$  - operating lever arm, in mm;  $r$  - drum radius, in mm;  $c$  - the distance from the insertion points of the belt to the joint, in mm;  $\mu$  - friction coefficient;  $\theta$  - enwrapping angle, in degrees.

## 2. Calculation of brake resistance

### 2.1 Preparation of brake resistance calculation with imposed design requirements

The calculation was divided into sections, such as joint areas of the assembly, connection areas of the band brake and brake body, weld seams or along the band brake. These calculation sections, shown in part, can be identified from the general scheme of the assembly, Figure 4. Table 1 shows the resistance calculation for the band brake drum.

Also, the resulting force at the end of the band of  $D-D$  section was calculated, Figure 5.a and the dimensioning of the thickness of the metal band was realized, where a higher value was chosen, Table 2. Similarly, the calculation of the tensile stresses found in  $E-E$  section of the band brake was realized; based on the data, a stress value far below the admisible stress resulted, Figure 5.b and Table 2.

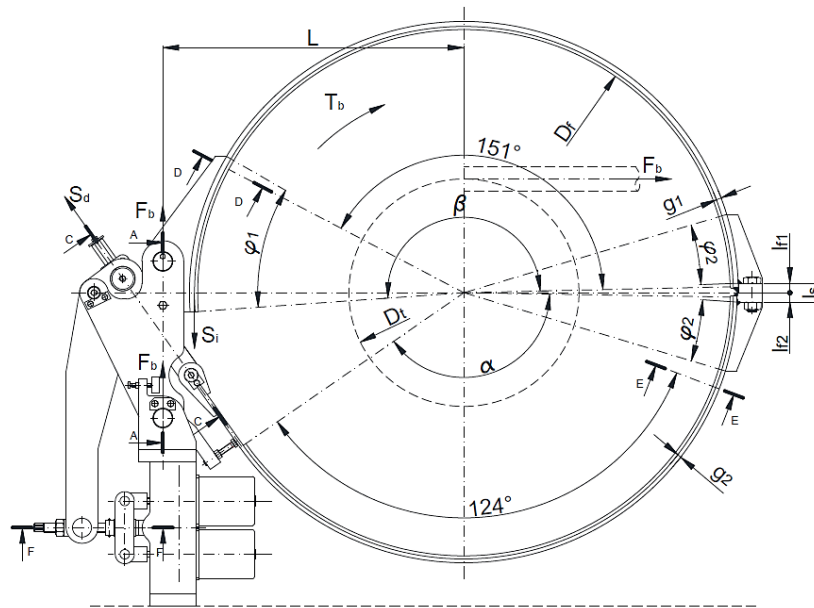


**Fig. 4.** Loading scheme of the system - 2D representation

**Table 1:** Calculation of the resistance of the drum on which the brake is placed [6,11,12]

Parameters	Symbol	Result
Cable diameter	$\varnothing$	76 mm
Drum diameter after one enwrap of the cable	$D_t$	726 mm
Braking force for a cable enwrap	$F_t$	1 000 000 N
Brake diameter	$D_f$	1.68 m
Brake friction coefficient	$\mu$	0.35
Contact angle of the lower band	$\alpha$	144°
Contact angle of the upper band	$\beta$	173°
Total contact angle	$\varphi = \alpha + \beta [^\circ]$ (2)	317°
Braking moment	$T = \frac{F_f \cdot D_t}{2} [N \cdot m]$ (3)	363 000 N·m
The maximum force exerted at the end of the band	$S_i = \frac{2 \cdot T \cdot e^{\mu \cdot \varphi}}{(e^{\mu \cdot \varphi} - 1) \cdot D_f} [N]$ (4)	504 967.23 N
The minimum force exerted at the end of the band	$S_d = \frac{2 \cdot T}{(e^{\mu \cdot \varphi} - 1) \cdot D_f} [N]$ (5)	72 824.38 N

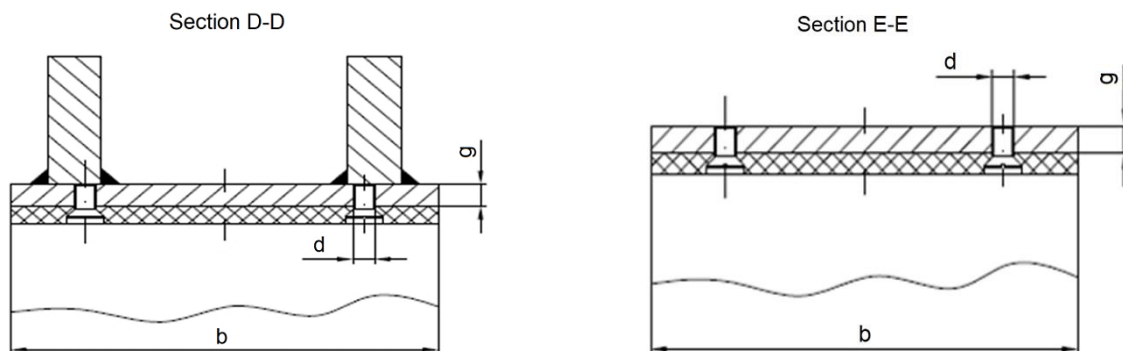


**Fig. 5.** D-D (a) and E-E (b) sections of the band brake [6,11,12]

**Table 2:** Calculation of band stretching in *D-D* and *E-E* sections [6, 11]

<b><i>D-D</i> section</b>		
<b>Parameters</b>	<b>Symbol</b>	<b>Result</b>
Contact angle of the band in <i>D-D</i> section	$\varphi_x = \alpha + 151^\circ$ [°] (6)	295°
Band braking force in <i>D-D</i> section (Euler)	$S_x = S_d \cdot e^{\mu \cdot \varphi_x}$ [N] (7)	441 466.96 N
The number of holes in the band in <i>D-D</i> section	$i$	2
The diameter of the holes in the band	$d$	10 mm
The width of the metal band	$b$	200 mm
The yield stress of the band material	$R_{eH(S355J2)}$	345 N/mm <sup>2</sup>
Tensile safety factor	$c$	0.8
The thickness of the metal band	$g \geq \frac{S_x}{(b - i \cdot d) \cdot c \cdot R_{eH(S355J2)}}$ [mm] (8)	8.89 mm
Selected thickness of the band	$g$	12 mm
<b><i>E-E</i> section</b>		
<b>Parameters</b>	<b>Symbol</b>	<b>Result</b>
Contact angle of the band in <i>E-E</i> section	$\varphi_{x_i}$	124°
Band braking force in <i>E-E</i> section (Euler)	$S_{x_i} = S_d \cdot e^{\mu \cdot \varphi_{x_i}}$ [N] (9)	155 325.61 N
Area of the <i>E-E</i> section	$A = b \cdot g - (i \cdot d)$ [mm <sup>2</sup> ] (10)	2160 mm <sup>2</sup>
Tensile stress in <i>E-E</i> section	$\sigma_t = \frac{S_{x_i}}{A}$ $\left[ \frac{\text{N}}{\text{mm}^2} \right]$ (11)	71.91 N/mm <sup>2</sup>
Admissible stress	$\sigma_{at} \leq c \cdot R_{eH(S355J2)}$ $\left[ \frac{\text{N}}{\text{mm}^2} \right]$ (12)	276 N/mm <sup>2</sup>

A calculation of the welds was made which combines the lugs at the end of the band brake to it. The contact area between the weld and the metal band part of the band brake was defined and the shear stress generated in the weld area was calculated, which stress was compared with the admissible value. From Table 3, it can be seen that the calculated stress value is half of the allowable stress, which indicates a safe operation.

**Table 3:** Calculation of the weld between the metal band and the lugs of the strip [6, 11]

<b>Parameters</b>	<b>Symbol</b>	<b>Result</b>
The outer radius of the band	$R_b$	866 mm
The angle of the weld	$\varphi_s$	0.59 mm
Lug thickness	$l_s$	25 mm
Weld thickness	$G_s$	7 mm
The contact surface between the weld and the metal band in <i>E-E</i> section	$A = 2 \cdot (R_b \cdot \varphi_s \cdot G_s) + 2 \cdot (l_s \cdot G_s)$ [mm <sup>2</sup> ] (13)	7 544.53 mm <sup>2</sup>
Calculated shear stress for one lug	$\tau_{t_s} = \frac{S_i}{A}$ $\left[ \frac{\text{N}}{\text{mm}^2} \right]$ (14)	66.93 N/mm <sup>2</sup>
Shear safety factor	$c$	0.35
Admissible shear stress	$\tau_{a_s} \leq c \cdot R_{eH(S355J2)}$ $\left[ \frac{\text{N}}{\text{mm}^2} \right]$ (15)	120.75 N/mm <sup>2</sup>

The entire brake system assembly has 10 bolts, each part having its established dimensions. In the paper, resistance calculations were performed for two of them. Thus, in Figure 6 and Table 4, bolt 7 is represented with the input data.

Table 4: Dimensioning of the bolt 7 [6, 11]

Parameters	Symbol	Result
Distance between bolt 7 and bolt 8	$a$	100 mm
Distance between bolt 7 and bolt 9	$b$	750 mm
Diameter of bolt 7	$d_5$	40 mm
The thickness of the lug of the stake	$S_2$	25 mm
Lever lug thickness	$S_5$	15 mm
The distance between the stake and the lever	$\delta$	1.5 mm
The distance between the lugs of the lever	$l_2$	55 mm
The yield stress of the bolt material	$R_{eH}(X20CrNi 17.2)$	650 N/mm <sup>2</sup>
Lever lug material yield stress	$R_{eH}(S355J2)$	345 N/mm <sup>2</sup>
Bending safety factor	$c$	0.8

Calculations for bending, shearing and contact pressure of bolt 7 are shown in Table 5 and verification of the diameter of bolt 7 in bending, shearing and contact is shown in Figure 7. From calculations, values much lower than the admissible ones can be observed, resulting a good bolt sizing. Also, bolt 8 was subjected to bending, shearing and contact pressure stresses, as represented in Figure 8 and Table 6. It is observed that the diameters resulting from the calculations are smaller than the diameter chosen in the design.

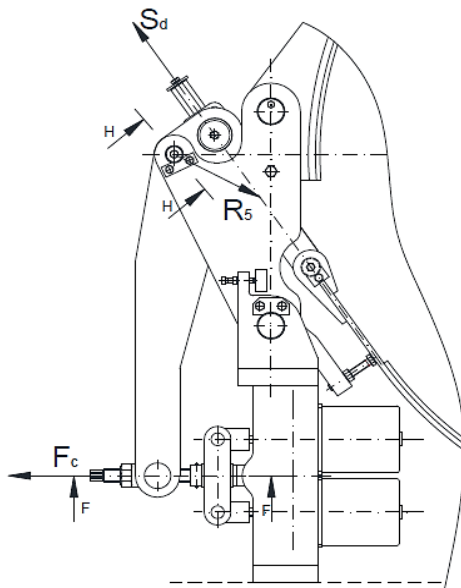


Fig. 6. Graphical representation of input data of bolt 7 [6, 11]

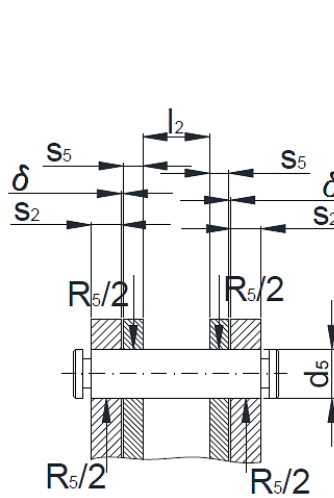


Fig. 7. Verification of diameter of bolt 7 in bending, shearing and contact [6, 11]

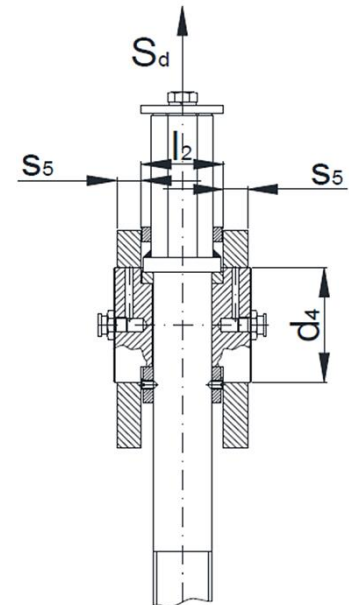


Fig. 8. Verification of diameter of bolt 8 in bending, shearing and contact [6, 11]

Table 5: Calculation of bending, shear and contact pressure of bolt 7 [6, 11]

Parameters	Symbol	Result
The force generated on the rod thread by the pneumatic system	$F_c = \frac{S_d \cdot a}{b} [N]$ (16)	9 709.92 N
$R_5$ force felt in the bolt	$R_5 = \frac{F_c \cdot (a+b)}{a} [N]$ (17)	82 534.29 N

Bolt bending moment	$M_{i_{max}} = \frac{R_5 \cdot (S_2 + S_5 + 2 \cdot \delta)}{4} \left[ \frac{\text{N}}{\text{mm}^2} \right]$ (18)	887.24 N/mm <sup>2</sup>
Polar moment of inertia	$W_p$	12 566.37 mm <sup>3</sup>
Moment of inertia	$W_z$	6 283.19 mm <sup>3</sup>
Resulting bending stress	$\sigma_i = \frac{M_{i_{max}}}{W_z} \left[ \frac{\text{N}}{\text{mm}^2} \right]$ (19)	141.21 N/mm <sup>2</sup>
Admissible bending stress	$\sigma_{at} = c \cdot R_{eH(X20CrNi 17.2)} \left[ \frac{\text{N}}{\text{mm}^2} \right]$ (20)	520 N/mm <sup>2</sup>
Resulting bending stress	$\sigma_{ai} \leq \sigma_{at} = c \cdot R_{eH(X20CrNi 17.2)} \left[ \frac{\text{N}}{\text{mm}^2} \right]$ (21)	141.21 N/mm <sup>2</sup> ≤ 520 N/mm <sup>2</sup>
Bolt diameter resulting from shear stress	$d_5 \geq \sqrt{\frac{4 \cdot R_5}{\pi \cdot c \cdot R_{eH(X20CrNi 17.2)}}}$ [mm] (22)	21.49 mm
Diameter of the resulting bolt resulting from the contact pressure	$d_5 \geq \frac{R_5}{2 \cdot S_5 \cdot c \cdot R_{eH(S355J2)}}$ [mm] (23)	9.97 mm
Minimum outer radius of lugs	$R \geq \frac{R_5}{4 \cdot S_5 \cdot c \cdot R_{eH(S355J2)}} + \frac{d_5}{2}$ [mm] (24)	24.98 mm
The chosen radius of the lugs	$R$	45 mm

**Table 6:** Calculation of bending, shear and contact pressure of bolt 8 [6, 11]

Parameters	Symbol	Result
Lever lug thickness	$S_5$	15 mm
The distance between the lugs	$l_2$	55 mm
Bolt material yield stress	$R_{eH(X20CrNi 17.2)}$	650 N/mm <sup>2</sup>
Lug material flow stress	$R_{eH(S355J2)}$	345 N/mm <sup>2</sup>
Bending safety factor	$c$	0.8
Admissible bending stress	$\sigma_{at} = 0.8 \cdot R_{eH(X20CrNi 17.2)} \left[ \frac{\text{N}}{\text{mm}^2} \right]$ (25)	520 N/mm <sup>2</sup>
Maximum bending moment	$M_{i_{max}} = \frac{S_d \cdot l_2}{4}$ [N·m] (26)	1 001 335.17 N·m
Dimensioning of the bolt according to the bending moment	$d_4 \geq \sqrt[3]{\frac{32 \cdot M_{i_{max}}}{\pi \cdot c \cdot R_{eH(X20CrNi 17.2)}}}$ [mm] (27)	26.97 mm
Shear safety factor	$c$	0.35
Bolt sizing as a function of shear stress	$d_4 \geq \sqrt[3]{\frac{4 \cdot S_d}{\pi \cdot c \cdot R_{eH(X20CrNi 17.2)}}}$ [mm] (28)	20.19 mm
Existing bolt diameter	$d_4$	75 mm
Safety factor at contact pressure	$c$	0.5
Admissible stress at contact pressure between bolt and lever	$\sigma_{at} = c \cdot R_{eH(S355J2)} \left[ \frac{\text{N}}{\text{mm}^2} \right]$ (29)	172.5 N/mm <sup>2</sup>
Lever lug thickness resulting from contact pressure	$S_5 = \frac{S_d}{2 \cdot d_4 \cdot \sigma_{at}}$ [mm] (30)	2.81 mm

Table 7 shows the calculation of the force generated at the level of the coils of the two M30 screws that join the lower band brake to the upper one in order to form the band brake subassembly.

**Table 7:** Strength calculation of M30 screws in the metal band joint area [6, 11]

Parameters	Symbol	Result
Contact angle of the upper band	$\varphi_{x_2}$	137°
Force between the bands	$S_{x_2} = S_d \cdot e^{\mu \cdot \varphi_{x_2}} \text{ [N]}$ (31)	168 163.40 N
Force applied to a screw	$F_{screw} = \frac{S_{x_2}}{2} \text{ [N]}$ (32)	84 081.70 N

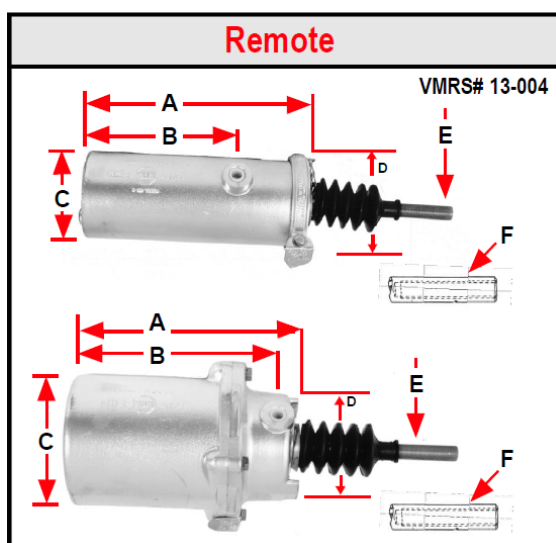
Also, in table 8, the welds in the joining area of the two bands were calculated. It can be seen that the values resulting from the calculations are much lower than the admissible values, which indicates that the area will resist at the imposed stresses.

**Table 8:** Calculation of the weld of the joining area of the two bands [6, 11]

Parameters	Symbol	Result
The development angle of a weld	$\varphi_2$	15°
The lug thickness of the band joint	$s_3$	30 mm
Radius of the weld	$X$	866 mm
Weld thickness	$a$	7 mm
The contact surface between the weld and the brake bands	$A = 2 \cdot (X \cdot \varphi_2 \cdot a) + (s_3 \cdot a) \text{ [mm}^2\text{]}$ (33)	3 384.06 mm <sup>2</sup>
Shear stress in the weld zone	$\tau_{ts} = \frac{S_{x_2}}{A} \left[ \frac{\text{N}}{\text{mm}^2} \right]$ (34)	49.69 N/mm <sup>2</sup>
Shear safety factor	$c$	0.35
The yield stress of the joint material	$R_{eH(S355J2)}$	345 N/mm <sup>2</sup>
Permissible shear stress	$\tau_f \leq c \cdot R_{eH(S355J2)} \left[ \frac{\text{N}}{\text{mm}^2} \right]$ (35)	120.75 N/mm <sup>2</sup>

## 2.2 Selection of the pneumatic actuation cylinder

The model of the chosen pneumatic cylinder is R5AHD, 5005 series, Figure 9, with the specifications shown in the table [8].



Series/ Model	5005/ R5AHD
Size	4
Stroke [inch]	4.37
20" rod	N/A
15" rod	5005012
7" rod	5005014
A [inches]	10.5
B [inches]	9.38
C [inches]	6.12
D [inches]	5.12
E [inches]	3/4" - 16UNF x 10.75"
F [inches]	1/2" - 20UNF x 3.00"
Inputs	3/8" - NPTF

**Fig. 9.** R5AHD-5005 pneumatic cylinder gauge dimensions and specifications [8]

The maximum developed force is calculated with the relation [9, 10]:

$$F = \frac{\pi \cdot d_{piston}^2}{4} \cdot p \text{ [N]}. \quad (2)$$

The pneumatic cylinder develops a maximum pressure,  $p$ , of  $p=85$  psi, equivalent to  $0.586$  Pa. The diameter of the cylinder piston,  $d_{piston}$ , is  $d_{piston} = 155$  mm. After calculations, it follows:

$$F = \frac{\pi \cdot 155^2}{4} \cdot 0.586 = 11057.345 \text{ N}. \quad (3)$$

The band brake is actuated by two cylinders mounted in parallel, the force required for braking being half of the combined load of the two cylinders.

### 3. FEM analysis of the braking system

Modeling of the band braking system was done using *Autodesk Inventor* software, Figure 10. Based on this modeling, finite element method (FEM) simulations were performed in *Ansys Workbench* program for both static and dynamic analysis.

The geometry of the system made in *Autodesk Inventor* was exported as a \*.stp file, followed to be imported into *Ansys Workbench* program [13,14,15,16,17,18].



**Fig. 10.** Graphical modeling of the pneumatic braking system for industrial winches

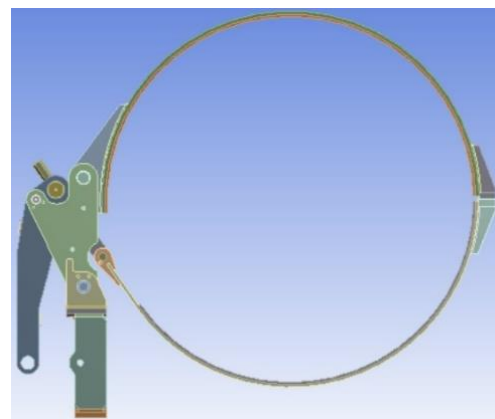
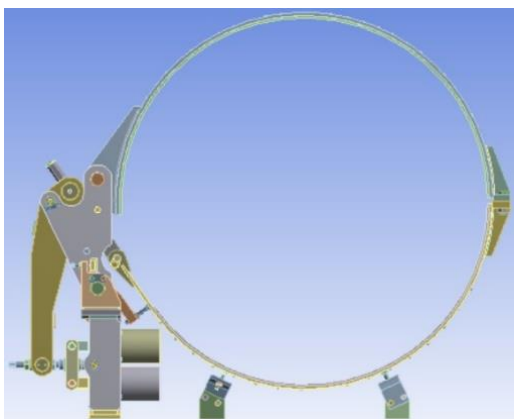


**Fig. 11.** Braking system imported into *Ansys Workbench*: original model (a) and simplified model (b) The complex geometry of the band braking system has been simplified to be able to perform a static calculation under the conditions of an acceptable solid finite element discretization, Figure 11. Being a complex structure, the discretization was realized using the *Patch Conforming* method, setting the side of the element to 1 cm. Under these conditions, a network with 438.504 nodes and 259.891 elements was obtained. The *SOLID187* element [17] was used in discretization, Figure 12. The steel used for the finite element calculation has the following mechanical properties [17]:

- Longitudinal Young's modulus,  $E=2.1 \cdot 10^{11}$  [N/m<sup>2</sup>];
- Poisson's ratio,  $\nu=0.3$ ;
- Density,  $\rho=7850$  [kg/m<sup>3</sup>];
- Yield stress,  $\sigma_y=350$  [MPa].

The boundary conditions imposed on the system are connection type conditions, respectively loads and links type conditions. Due to the specifics of the system addressed, in addition to contact conditions, *Revolute-joint*, *body-body* and *body-ground* conditions were imposed. *Revolute-joint* and *body-body* conditions were applied to the assembly joints and the *body-ground* connection to the inner face of the band brake and simulates the contact between the drum and the band brake. The load is imposed by applying the braking moment in the *revolute body-ground joint*. Fixing the system is done on the lower face of the braking support, indicated by label A, Figure 13.

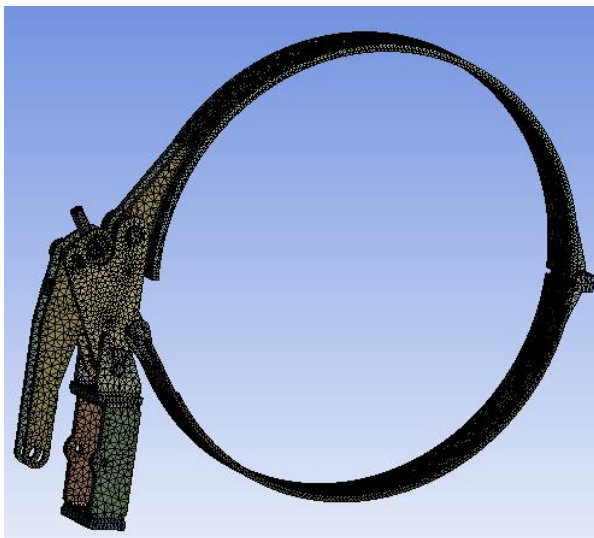


**Fig. 12.** Mesh of the system

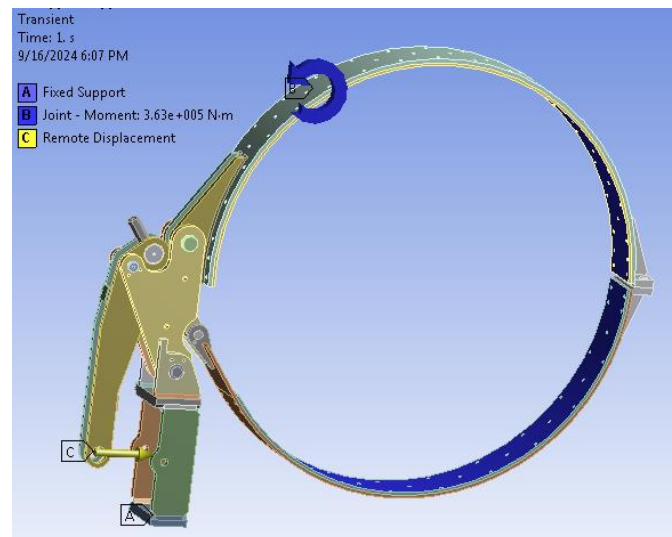


**Fig. 13.** Boundary conditions imposed to the system

The actuation of the braking lever is achieved by applying the *Remote Displacement* condition, which equates the action of the two pneumatic motors; the reaction in this connection is the very force necessary for the system's stationarity condition. The used material has linear properties and behavior but due to the large displacements and contact conditions as well as the *joint* conditions present, the solution requires a non-linear approach with increasing loading.

Figure 14 shows the von Mises stress distribution for the static analysis, with the maximum value concentrated in the weld seam of the braking support. It should be noted that the maximum stress does not exceed the flow value.

The distribution of the maximum shear stresses occurring in the structure is presented in Figure 15. A distribution similar to the von Mises stresses can be observed, the value being half of the maximum value of the stresses.

The distribution of total displacements is shown in Figure 16. The system is of an organological type, with small displacements and high stresses, the maximum displacement being the imposed one.

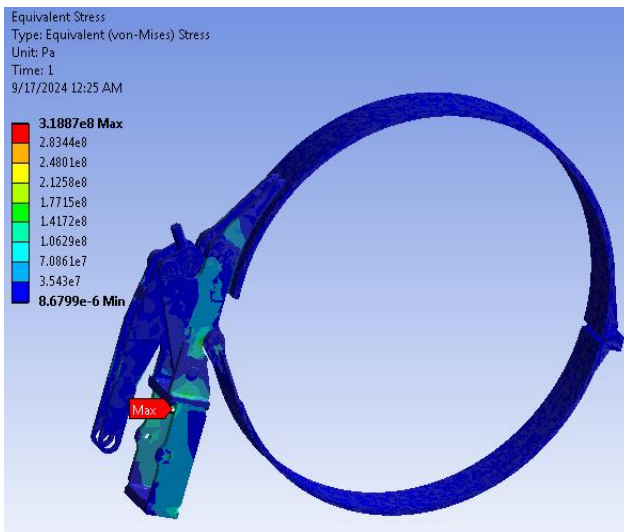


Fig. 14. Equivalent von Mises stress distribution

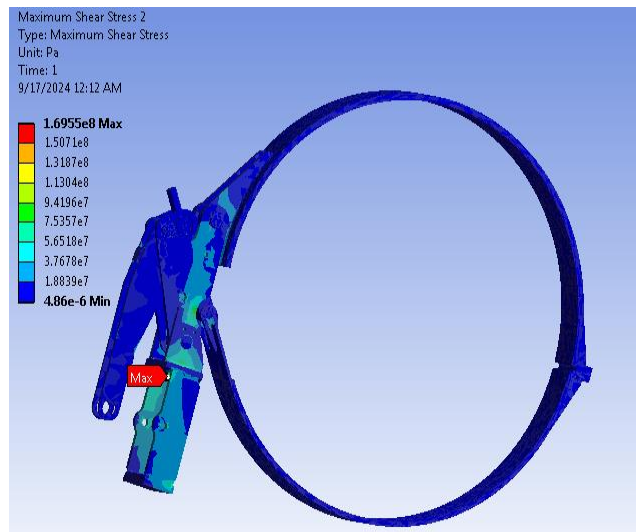


Fig. 15. Maximum shear stress distribution

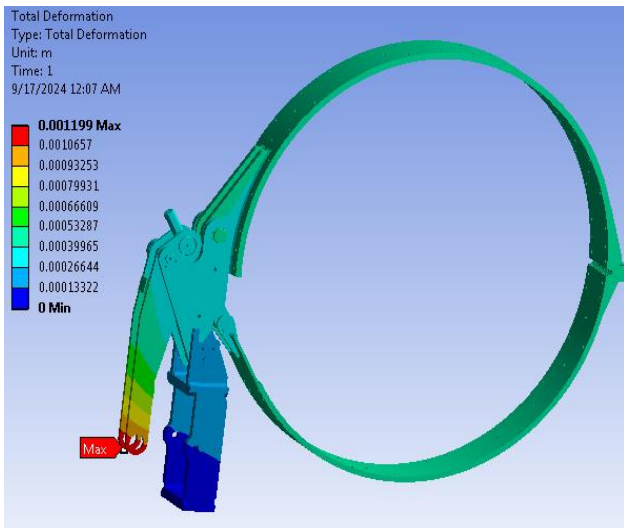


Fig. 16. Total displacement distribution

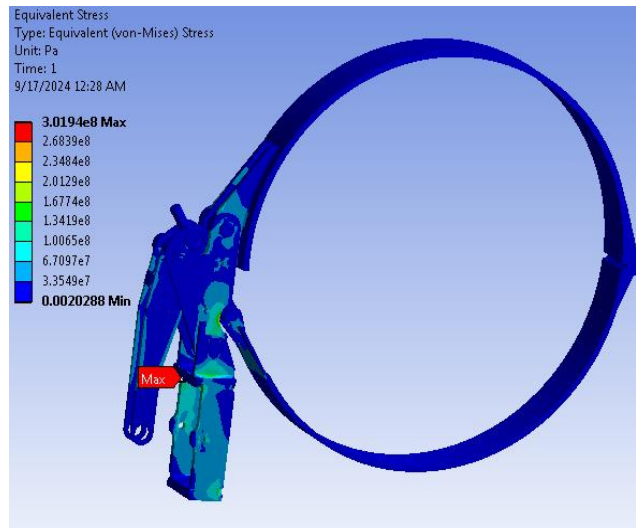


Fig. 17. Equivalent von Mises stress distribution

A global estimate of the stress state in relation to the yield stress of the material is achieved by the distribution of the safety factor over the entire system. The safety factor has values above 1 in the maximum von Mises stress zone, at the dynamic analysis, Figure 17.

The system works in stationary mode. As such, a static calculation is suitable for finite element strength analysis.

In the assumption of a shock actuation, the system is analyzed in dynamic mode, using the *Transient Structural* module of the *Ansys Workbench* program.

In order to make this calculation, a system braking time of 1 second was imposed, a condition that will introduce the phenomenon called "shock" into the system.

The *Transient* module works differently from the *Static Structural* analysis module, the difference being the way to obtain the numerical solution. In the case of the *Static Structural* module, the values of displacements in each node are calculated at the same time, while in the *Transient Structural* module, the values of displacements, velocities and accelerations are calculated and transmitted from node to node, starting with the loading area. The von Mises stress distribution in the system, resulting from the dynamic calculation, is identical to that obtained from the static analysis, Figure 17, the only significant difference being the decrease of the maximum stress by about 20 MPa.

The previously mentioned notion of "shock" is expressed by a sudden increase in the accelerations concentrated in the actuation area of the pneumatic cylinders, followed by a rapid decrease to 0 and a uniform distribution in the system.

Figure 18 shows the distributions of the accelerations at the time of actuation of the pneumatic cylinders (the moment of the shock) and the distribution at the end of the analysis.

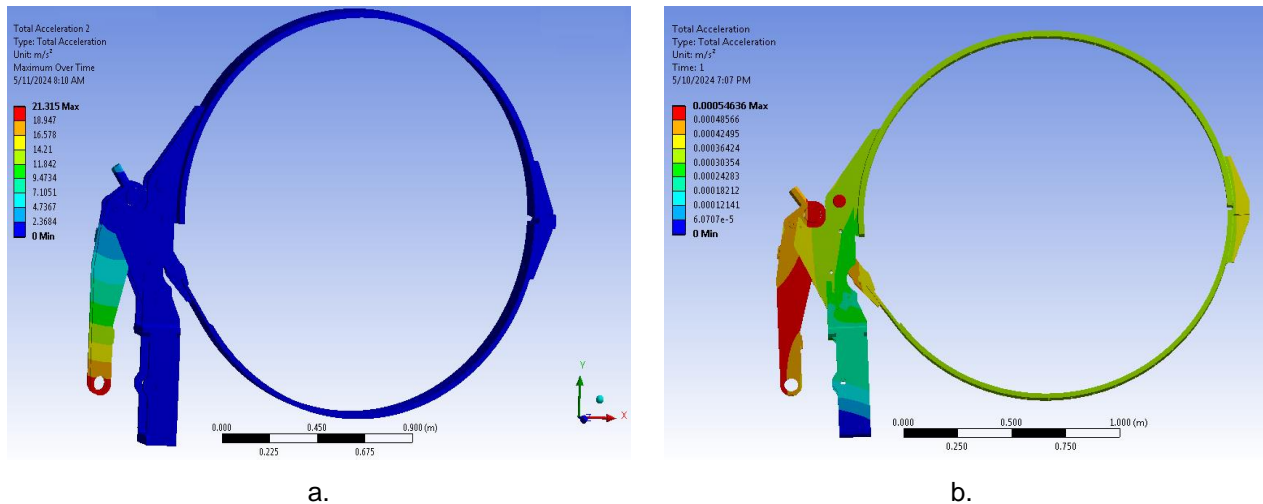


**Fig. 18.** The distribution of accelerations at the time of actuation of the pneumatic cylinders (a) and at the end of the dynamic analysis (b)

The appropriate results of the two types of analysis indicate that a static analysis is sufficient to obtain a suitable solution from the point of view of strength calculation.

The value of the initial accelerations, as shown in Figure 18.a, is about 22 m/s<sup>2</sup>, a very high and dangerous value for a long operation of the system. However, the system operates around this value for a short period of time, as previously shown; in the case of long-term operation of the system around this value, a very high wear rate results, leading to a destruction of the braking system in a short period of time.

The von Mises stresses, whose distribution is shown in Figure 14 for static calculation and Figure 17 for dynamic calculation, show values of about 319 MPa and 301 MPa. These values are below the flow level of the material from which the parts are made, which indicates a good exploitation of the entire system. Therefore, these factors lead to high reliability.

It can be seen that the von Mises stress concentration zone is located around the brake support, which is imposed by the designer because this part has a simple and very robust geometry and is also welded directly to the shipboard to allow unloading of the whole system in the ship in order to dissipate the tensions.

From the value of the shear stresses shown in Figure 15 (about 170 MPa), a value that is much lower than that of the von Mises stresses, it is understood that the system does not present danger zones from the point of view of these types of stresses.

#### 4. Conclusions

In the paper, a study was presented regarding the band braking system in the structure of industrial winches. Aspects related to the modeling of the band braking system in *Autodesk Inventor* program were presented, as well as the way to transfer this model to the finite element analysis - *Ansys Workbench* program. The results of the analysis were presented as distributions of displacements and maximum von Mises stresses, maximum shear stresses, including the static safety factor (established in relation to the yield stress of the material).

In addition to the static analysis, a dynamic analysis was also performed when the braking system was actuated for 1s.

The results of this analysis justify performing only a static calculation, because the stress level in the two simulations (static - with *Static Structural* module and dynamic - with the *Transient Structural* module) is the same.

Analytical calculations were also realized for the most important connections in the band brake structure starting from the moment to be overcome at the actuation forces from the pneumatic cylinders. Analysis of the state of stresses and strains in the deterministic approach (with material properties and fixed value loads) for organological structures reveals small displacements and strains, but high stresses, often close to the yield stress of the material. For such systems, static analysis using the finite element method can provide a global assessment of the stress and strain state. The band brake studied in *Ansys Workbench* program, which represents a complex system, includes specific connection elements (*joint* type) and contact conditions that require the calculation with finite elements in large displacements (non-linear calculation, even if the mechanical properties of the material are considered in the linear-elastic domain).

## References

- [1] Kisiel, M., D. Szpica, J. Czaban, and H. Köten. "Pneumatic brake valves used in vehicle trailers - A review." *Eng. Fail. Analysis* 158 (2024): 107942.
- [2] Wang, X., D. Geng, L. Zhang, W. Xu, H. Peng, and G. Sun. "Structure and function experiment of pneumatic ring brake." Paper presented at the 2021 International Conference on Mechanical Design (2021 ICMD), Changsha, China, August 11-13, 2021. *Mechanisms and Machine Science* 111 - Advances in Mechanical Design (2022): 881-890.
- [3] Knott. "Band brake systems & solutions". Accessed September 17, 2024. <https://knottbrake.com/categories/band-brakes>.
- [4] SEA HydroSystems. "The role of hydraulic brakes in modern heavy machinery". May 30, 2024. Accessed September 16, 2024. <https://seahydrosys.com/heavy-machinery-hydraulic-brakes-guide>.
- [5] Alterous. "Band brakes". Accessed September 17, 2024. <https://www.alterous.com/products/industrial-applications/brakes/band-brakes>.
- [6] DMT Marine Equipment. Products. Accessed September 17, 2024. <https://www.dmt-winches.com>.
- [7] EMCÉ Winches. "Winch calculation". Accessed September 20, 2024. <https://emce.com/about-winches/winch%20calculation>.
- [8] FindItParts. Brake system service. Accessed September 17, 2024. <https://www.finditparts.com/products/394230/mgm-5004013>.
- [9] Baroiu, N., and G.A. Moroşanu. *Hydraulic Drive Systems/Sisteme de acţiune hidraulică*. Galati, Academica Publishing House, ISBN 978-606-606-011-0, 2022.
- [10] Teodor, V.G., V. Păunoiu, N. Baroiu, and F. Susac. "Optimization of the measurement path for the car body parts inspection" *Measurement* 146 (2019):15-23.
- [11] Beznea, E.F. *Material strength. Simple loads. Problems and tests/Rezistenţa materialelor. Solicitări simple. Probleme şi teste*. Galati, Galati University Press, 2018.
- [12] Iglesias-Baniela, S., and J.M. Pérez-Canosa. "Spring-loaded winch band brakes as tools to improve safety during mooring operations on ships." *The International Journal on Marine Navigation and Safety of Sea Transportation* 14, no. 3: (2020): 711-719.
- [13] Autodesk. Products. Accessed September 17, 2024. <https://www.autodesk.com>.
- [14] Moroşanu, G.A., N. Baroiu, V.G. Teodor, V. Păunoiu, and N. Oancea. "Review on study methods for reciprocally enwrapping surfaces." *Inventions* 7, no. 1 (2022): 10.
- [15] Baroiu, N., G.A. Moroşanu, V.G. Teodor, and N. Oancea. "Roller profiling for generating the screw of a pump with progressive cavities." *Inventions* 6, no. 2 (2021): 34.
- [16] Teodor, V.G., N. Baroiu, and F. Susac. *The synthesis of new algorithms for CAD profiling of cutting tools*. Saarbrücken, Lambert Academic Publishing, ISBN 978-613-7-08923-1, 2018.
- [17] Ansys. Products. Accessed September 17, 2024. <https://www.ansys.com/products/ansys-workbench>.
- [18] Belabend, S., V. Păunoiu, N. Baroiu, R. Khelif, and I. Iacob. "Static structural analysis analytical and numerical of ball bearings." Paper presented at the 6th International Conference on Advanced Manufacturing Engineering and Technologies - NEWTECH 2020, Galati, Romania, September 9-11, 2020. *IOP Conference Series: Materials Science and Engineering* 968 (2020): 012026.